Polymer 240 (2022) 124488

Contents lists available at ScienceDirect

Polymer

journal homepage: www.elsevier.com/locate/polymer

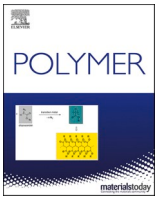

Encapsulation of cellulose nanocrystals into acrylic latex particles via miniemulsion polymerization

Ezgi M. Dogan-Guner [a], F. Joseph Schork [a], Stan Brownell [b], Gregory T. Schueneman [c], Meisha L. Shofner [d], J. Carson Meredith [a,*]

[a] School of Chemical and Biomolecular Engineering, Georgia Institute of Technology, Atlanta, GA, USA
[b] Dow Coating Materials, The Dow Chemical Company, Collegeville, PA, USA
[c] Forest Products Laboratory, U.S. Forest Service, Madison, WI, USA
[d] School of Materials Science and Engineering, Georgia Institute of Technology, Atlanta, GA, USA

ARTICLE INFO

Keywords:
Encapsulation
Miniemulsion polymerization
Cellulose nanocrystal
Acrylic monomers
Surface modification
Functionalization

ABSTRACT

Cellulose nanocrystals (CNCs) show promise for enhancing properties of waterborne latexes and coatings. Miniemulsion polymerization is a promising route to obtaining well-controlled latex distributions sufficient to encapsulate CNCs in the monomer phase. Here, we demonstrate the first miniemulsion polymerization resulting in encapsulation of CNCs that incorporates costabilizer, water soluble initiator, and comonomer mixtures, aspects that are important for practical implementation. CNCs were added to the monomer phase as either unmodified (umCNC) or one of two functionalized forms: modified with isocyanatoethyl methacrylate (mCNC, containing a polymerizable vinyl group) or grafted with butyl acrylate/methyl methacrylate copolymer (gmCNC). The gmCNCs were incorporated successfully into acrylic particles. In contrast, the umCNCs were located outside the formed latex particles. Interestingly, the mCNCs coagulated during the polymerization, highlighting the challenge of utilizing polar and reactive acryloyl CNC surface modifiers that lead to migration from the droplet phase.

1. Introduction

Polymer colloids are essential precursors used in various industrial applications. These colloid systems have been used in the paper, leather, and construction industries and in printing inks, coatings (decorative, protective, automotive), and adhesives [1]. Interest in the research and applications of waterborne polymer colloids has increased in the last decades, as opposed to traditional solventborne technologies, since market and regulatory trends are moving more towards eco-friendly materials [2].

An aqueous polymer colloid or a latex is a dispersion of submicron polymer particles in water. The most commonly used method to produce latexes is conventional emulsion polymerization. Emulsion polymerization is a heterogeneous free radical polymerization where the monomer is initially contained in droplets stabilized by a colloidal stabilizer (typically surfactant) in water. Surfactants used above the critical micelle concentration (CMC) stabilize the monomer droplets (~10 μm) and also form micelles (~10 nm) in the aqueous phase [3]. Emulsion polymerization employs monomers having a slight water solubility and a water-soluble initiator to initiate the polymerization in the aqueous phase. Monomers diffuse from relatively larger monomer droplets to the aqueous phase to supply the polymerization that occurs in the continuous aqueous phase (homogeneous nucleation), in monomer-swollen micelles (micellar nucleation), or (very slightly) in the monomer droplets (droplet nucleation).

Miniemulsion polymerization is another route to synthesize latexes. Both conventional emulsion polymerization and miniemulsion polymerization result in polymer particles ranging from 50 to 500 nm; however, the mechanism for particle growth differs. Miniemulsions contain smaller (<1 μm) monomer droplets obtained by a high shear emulsification step and use a costabilizer to prevent Ostwald ripening. A low surfactant concentration is used so that no micelles form in the aqueous phase after the emulsification step. Reducing the droplet sizes increases the surface area for polymerization, enabling droplet nucleation to become the dominant mechanism for the growth of particles. The identity of droplets is maintained with an effective surfactant and costabilizer system during the polymerization. Whereas surfactants stabilize droplets against coalescence as in emulsion polymerization,

* Corresponding author.
E-mail address: carson.meredith@chbe.gatech.edu (J.C. Meredith).

https://doi.org/10.1016/j.polymer.2021.124488
Received 6 October 2021; Received in revised form 22 December 2021; Accepted 25 December 2021
Available online 27 December 2021

costabilizer (e.g., a long chain alkane or alcohol) retards monomer diffusion from small to large droplets (Ostwald ripening) in miniemulsions [4].

Miniemulsion polymerization is a favorable process for the encapsulation of small molecules and solids (fillers) in a polymer matrix to produce latexes with hybrid polymer particles [5]. Unlike in emulsion polymerization, the droplets act as "nanoreactors" for the polymerization, promoting the homogeneous distribution of fillers in the polymer particles. The droplet size can be controlled with the surfactant/costabilizer system, and the size is not affected by the polymerization parameters [6]. Research interest in producing latexes containing hybrid particles has increased since the early 2000s. The benefit offered by encapsulation processes varies depending on the nature of encapsulated material and the requirements of the application. Organic or inorganic materials have been incorporated into polymeric particles, for example, to protect the material from the environment, or to prevent the material from agglomerating in the continuous phase, or to inhibit the aggregation of the material during film formation, providing homogeneous distribution of the filler over the polymer film. Furthermore, in biomedical applications, encapsulation allows control over the release of drugs and curing agents [7].

Many researchers have studied the miniemulsion technique to encapsulate inorganic nanoparticles, including carbon nanotubes [8], carbon black [9], silica [10,11], titanium dioxide [12], iron oxide [13], and clay platelets [14]. Organic materials such as dyes and functional organic molecules have also been encapsulated via miniemulsion polymerization [15]. Many of the nanoparticle classes studied for encapsulation are hydrophilic. Therefore, surface functionalization has been performed for the hydrophilic nanoparticles to decrease their hydrophilicity and increase compatibility with monomers before the miniemulsification step.

Recently, an organic reinforcing phase that has attracted attention for encapsulation is cellulose nanocrystals (CNCs). CNCs are stiff nanomaterials derived from cellulose present in the cell wall of various plants and from other renewable sources. CNCs are typically extracted by sulfuric acid hydrolysis of cellulose fibers. Due to their renewable nature, crystallinity and high specific strength, CNCs have been incorporated into latexes to modify the barrier, mechanical or other properties of the resulting films [16,17]. However, because of their hydrophilicity, CNCs have been added to the aqueous phase of latexes, and either remain in the aqueous phase or adsorb on the surface of the particles. When CNCs are added to the aqueous phase of latex, CNC aggregates form in the polymer matrix, after the latex particles coalesce around the CNCs during film formation [16,17]. Encapsulating CNCs inside the latex particles could alleviate CNC aggregation in the polymer film (Fig. 1) and protects them from interfering in water-phase formulation chemistry, for example interfering with other charged species including salts and pigments.

Two publications have reported incorporating CNCs into polymer particles through emulsion or miniemulsion methods. The first study, by Kedzior et al. [18], demonstrated that surface-functionalized CNCs could be encapsulated inside poly(methyl methacrylate) (PMMA) latex particles. CNCs were grafted with poly(butyl acrylate) (PBA) by using surface-initiated atom transfer radical polymerization (SI-ATRP) and dispersed in methyl methacrylate (MMA) before the polymerization. The study reports a miniemulsion polymerization with an oil-soluble initiator and without using a costabilizer. While the authors did not note an increase in particle size, or change in size distribution, during the polymerization, the absence of costabilizer can shift the particle growth mechanism from that of miniemulsion polymerization to a microsuspension polymerization. As a result, miniemulsion polymerizations are nearly always carried out with a non-polar costabilizer, and most utilize water soluble initiators. The second study, by Yu et al. [19], functionalized CNCs with a silane coupling agent to integrate them into an acrylic pressure sensitive adhesive (PSA) system. A semi-continuous seeding emulsion polymerization was performed, and CNCs were found mainly anchored on the surface of acrylic particles. The resulting particle morphology improved the tack and peel strength of PSAs compared to the addition of native CNCs. To our knowledge, no work has reported attempts to carry out miniemulsion co-polymerizations with CNCs, where mixtures of comonomers are used or where the CNC had an active surface acryloyl group. This paper aims to explore these capabilities under conditions that are suitable for industrial implementation of miniemulsion polymerization, notably including the use of costabilizer and water soluble initiator. We seek to determine the relative effectiveness of modified CNC (mCNC) as a reactive comonomer that incorporates chemically into the growing droplet, versus grafted-modified CNCs (gmCNC) as physically incorporated fillers. A potential confounding factor to be explored is the ability of mCNC to remain partitioned into monomer phase droplets that contain a nonpolar costabilizer. Inefficient partitioning can include possible aqueous polymerization of free radical groups on CNCs if they migrate from the organic to water phase, interference with surfactant coverage of drops if CNCs migrate from the interior of organic phase drops to the water-droplet interface, and interactions with the initiator or transfer of active radicals to droplets in either case.

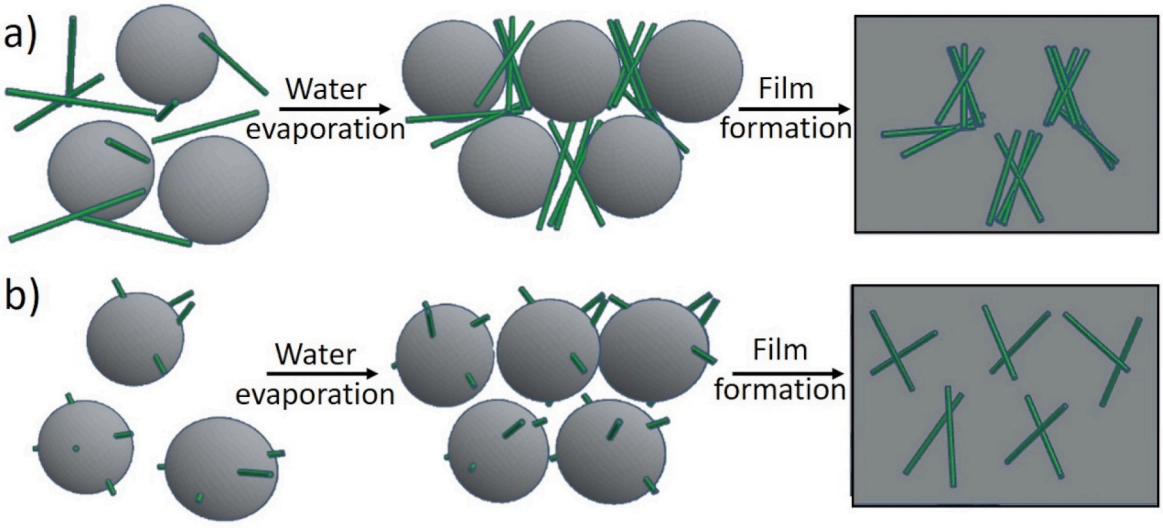

Fig. 1. Film formation process of waterborne polymeric particles with CNC located a) in the aqueous phase b) inside the latex particles.

To address these questions, we explored the incorporation of surface functionalized CNCs into poly(BA-MMA) copolymer latex particles with a miniemulsion polymerization technique. We modified the CNC surface by using isocyanatoethyl methacrylate (IEM) molecules and grafted poly (BA-MMA) copolymer via a *grafting through* [20] approach. We identified options for designing nanocomposite coatings by using the CNC surface functionalization and processing method to preferentially locate the CNCs within the formed composite structure and we explored challenges and limitations of the encapsulating approach.

2. Experimental section

2.1. Materials

Freeze-dried CNCs (with 1.06 wt% Sulfur) from the US Forest Service Forest Products Laboratory, Madison, WI were used as received. Dimethyl sulfoxide (DMSO, extra dry, ≥ 99.8%) was supplied in a 100 ml AcroSeal™ bottle from ACROS Organics. 2-isocyanatoethyl methacrylate (IEM, at >98% purity), dibutyltin dilaurate (DBTDL), methyl methacrylate (MMA - 99%, stabilized with MEHQ), benzoyl peroxide (BPO, Luperox® A98), inhibitor remover column, toluene (ACS, 99.5%), dimethylformamide (DMF, anhydrous, 99.8%), potassium persulfate (KPS, ACS reagent, ≥ 99%), sodium bicarbonate (ACS reagent, ≥ 99.7%), and hexadecane (HD - ReagentPlus®, 99%) were purchased from Sigma-Aldrich. Butyl acrylate (BA - >99%, stabilized with MEHQ) was obtained from TCI America. Sodium dodecyl benzene sulfonate (SDBS, POLYSTEP® A-16-22) was provided by Dow Coating Materials, The Dow Chemical Company, Collegeville, PA. Methyl methacrylate and butyl acrylate were passed through an inhibitor remover column (filled with basic alumina) before the polymerization.

2.2. Preparation of modified CNC (mCNC)

A sample of 0.1 g of unmodified CNCs (umCNCs) was mixed with 11 g anhydrous DMSO in a septum-sealed vial. The vial was clamped inside a bath sonicator (2510 Branson), and the mixture was sonicated for 30 min to promote the dispersion of umCNCs in DMSO. An empty two-neck round bottom flask was equipped with a magnetic stirrer, rubber stoppers, and needles punched through rubber septa on two necks. Then, the flask was submerged in an oil bath at 65 °C and a nitrogen stream was purged through the flask for 20 min to flush out oxygen. The bath-sonicated umCNC/DMSO dispersion was transferred from the septum-sealed vial to the heated reaction flask by using a syringe and a needle. In a separate vial, IEM and DBTDL were mixed and quickly added dropwise to the stirring umCNC/DMSO dispersion. The concentrations of IEM and DBTDL in DMSO were 5.7 wt% and 0.3 wt%, respectively. The mixture of umCNC/DMSO/IEM/DBTDL was magnetically stirred at 65 °C for 30 min under a nitrogen flow. The product dispersion was first mixed with toluene and centrifuged at 3000 rpm for 10 min to precipitate the modified CNC (mCNC). Then, the precipitated mCNC was mixed with acetone and centrifuged at 3000 rpm for 10 min (repeated 2 times) for purification. The collected mCNC was flash-frozen in liquid nitrogen and dried through lyophilization (Labconco FreeZone 4.5 L, with pressure <0.2 mbar, −55 °C of coil temperature) for 2 days.

2.3. Preparation of polymer-grafted modified CNC (gmCNC)

The starting material for polymer grafted mCNCs (gmCNCs) was the mCNC produced with the procedure explained in the previous section. Before the lyophilization step, the precipitated mCNC from the reaction medium was dispersed in 6 g of DMF as a first step in preparing the gmCNC. The mixture was transferred into a 50 ml round bottom flask. Benzoyl peroxide (5 mg) as the initiator, BA (1 g), and MMA (1 g) were added to the mixture. The flask was submerged into an oil bath and purged with a nitrogen flow for 15 min to remove oxygen. To facilitate polymerization, the mixture in the flask was stirred for 6 h in an oil bath at 70 °C. After the polymerization, the product solution in the flask were mixed with toluene and centrifuged to remove the free polymer in the solution. The gmCNCs settled to the bottom of the centrifuge tube because of density difference between gmCNC and free polymer in toluene. The purified gmCNC was recovered from the centrifuge tubes and dried in vacuum at 70 °C for 24 h.

2.4. Preparation of acrylic latexes

2.4.1. Controlling the particle size of the latex

Acrylic latexes were synthesized via miniemulsion polymerization. Aqueous and monomer phases of the miniemulsion were prepared based on the recipe given in Table 1. The monomer phase consisted of BA/MMA monomers and HD (the most common costabilizer in miniemulsion polymerization). For the aqueous phase, sodium carbonate (10 mM) and SDBS surfactant were mixed with ultra-pure water. To control the particle size in the latex as a function of surfactant concentration, neat latexes were prepared by using different amounts of SDBS in the aqueous phase. The initiator solution was prepared by dissolving the specified amount of KPS (10 mM) in 0.8 g ultra-pure water. The monomer phase was added to the aqueous phase, and the mixture was stirred for 20 min for pre-emulsification. Then, the mixture was ultrasonicated by using a probe sonicator (Q500, QSonica Ultrasonic Processor with a maximum power of 500 W) at 60% amplitude for 3 min in an ice bath. The miniemulsion was transferred to a 25 ml two-neck round bottom flask equipped with a magnetic stir bar. The flask was submerged in an oil bath and sealed with a condenser and a rubber septum. A nitrogen gas flow was provided through the rubber septum, and the condenser was connected to a recirculating bath (VWR) with a coolant temperature set to 2 °C (Fig. S1). The miniemulsion in the flask was bubbled and flushed with nitrogen gas flow for 10 min with the oil bath at ambient temperature. The oil bath temperature was set to 70 °C and the polymerization was allowed to progress for 7 h after injecting the initiator solution.

2.4.2. Incorporating CNCs into the latex

The miniemulsion polymerization procedure stated above was used with some changes to synthesize the latexes with CNCs. First, CNCs (umCNC, mCNC, or gmCNC) were dispersed in the monomer phase as either 0.5 wt% or 1 wt% of total monomer mass (based on *total* mass, not pure CNC mass). Second, two different surfactant concentrations (0.81 mM and 2.42 mM) were selected to synthesize the latexes since these surfactant concentrations resulted in latex particle sizes larger than the average length of CNCs. Third, the initiator concentration and polymerization temperature were increased and the polymerization time was decreased in order to improve the monomer conversion and minimize the coagulation. Also, the initiator solution was injected in two steps. Both the concentration of KPS and sodium carbonate were 20 mM in the aqueous phase instead of 10 mM. Half of the initiator solution was injected when the oil bath reached 85 °C, and polymerization was allowed to proceed for an hour. Then, the rest of the initiator solution was injected, and polymerization was carried out for two more hours. Neat latexes were also synthesized with the same polymerization conditions for comparison. After the polymerization, the latexes were

Table 1
Composition of the miniemulsion polymerization of BA/MMA latexes.

	Components	Mass and Concentration
Monomer phase	BA	1 g
	MMA	1 g
	HD	0.08 g
Aqueous phase	Water	8 g
	SDBS (10 wt% aqueous solution)	0.1–0.9 g (0.81–7.28 mM)
	KPS	0.02 g (10 mM)
	Sodium bicarbonate	Same as KPS

passed through a 200-mesh strainer. The latex coagulation was collected and dried for weight measurement. PTFE evaporating dishes having a diameter of 38 mm were used to cast the latex films (Fig. S2). 1.5 ml latex was added to the dish and vacuum-dried at 70 °C for 24 h. The thickness of the latex films was 200 ± 50 μm.

2.5. Characterization

The solid content of the latexes was determined gravimetrically, and monomer conversions were calculated by using equation (1) where C is the measured monomer conversion, $S_{measured}$ is the measured percent solids in the latex, $S_{non-polymer}$ is the percent non-polymer solids calculated from the recipe, and S_{100} is the percent total solids calculated from the recipe assuming 100% conversion.

$$C\ (\%) = 100 * \frac{S_{measured} - S_{non-polymer}}{S_{100} - S_{non-polymer}} \quad (1)$$

The pH of the latexes was measured by using a Mettler Toledo Seven2Go pH/mV meter equipped with Semi-Micro L pH electrode.

Zeta potential and average particle size of latexes were measured by using a Malvern Zetasizer Nano ZS90. The latexes were diluted with DI water to 0.025 wt% for both zeta potential and size measurements. The average of three measurements was reported.

A Ramé-Hart goniometer was used to perform water contact angle measurements of CNC samples and surface tension measurements of the latexes. For contact angle samples, 1 wt% suspensions of umCNC, mCNC and gmCNC were prepared in DMSO, and the CNC suspensions were drop-cast on glass slides and vacuum-dried (60 °C - 24 h). Five deionized water droplets (10 μl) were placed on each sample. The water contact angles were measured 60 s after the water droplets were dispensed. For surface tension measurements, 1 ml of latex was withdrawn by using a microsyringe with a stainless-steel needle. The microsyringe was mounted to the instruments and surface tension was measured from a pendant drop of the latex.

Attenuated total reflectance Fourier transform infrared (ATR-FTIR) spectroscopy was performed on CNC samples and latex films. A Nicolet 6700 FTIR spectrometer equipped with a diamond crystal single bound ATR attachment was used to obtain spectra with a resolution of 4 cm^{-1} and 64 scans at a range of 4000–650 cm^{-1}. The spectra were normalized at the 1060 cm^{-1} peak associated with the C–O vibration of the third carbon.

Elemental analysis was carried out by Atlantic Microlab (Norcross, GA) with combustion method using automatic analyzers. C, H, N and S contents of the CNC samples and the latex samples were analyzed. The results were used to calculate the degree of substitution of IEM in mCNC, grafting density and the copolymer composition of the grafted polymer in gmCNC.

Thermogravimetric analysis (TGA - Q50, TA Instruments) was performed for thermal stabilities and degradation patterns of CNC samples. The samples were heated from 25 °C to 600 °C under nitrogen atmosphere with a heating rate of 10 °C/min.

The morphology of CNCs and latex particles were imaged by atomic force microscopy (AFM – Bruker Dimension Icon) in tapping mode. umCNC and mCNC dispersions in DMSO at a concentration of 1 wt% were diluted to approximately 0.001 wt% and drop-cast onto a piranha etched silicon wafer. A probe (HQ:NSC14/No Al-15) with a resonance frequency of 160 kHz and a force constant of 5 N/m was used to capture the images. We used Gwyddion software to analyze the height images for the size distributions of CNCs. The length and height of 50 isolated particles were measured from multiple height images. The length was measured as the distance between two intersections in the height profile of an individual CNC across its length. The tip convolution effects for length measurements were corrected by assuming the cross section of the CNC to be circular [21]. The height was measured as the distance between the highest point across its length and the surface of the substrate. The height measurements were not corrected because tip convolution effects are negligible for the height values [22].

Partition tests were performed to study the preference of CNCs to aqueous phase or monomer phase. Monomer/water mixtures were prepared in 7 ml glass vials. The monomer – water ratio was 1:4 as used in miniemulsion polymerizations. Monomers containing 50 wt% BA and 50 wt% MMA were mixed with different types of CNCs (umCNC, mCNC, and gmCNC) at a concentration of 1 wt% in separate vials. DI water was added to the monomer mixtures and partition of CNCs was observed during 24 h as compared to the case where we mixed only monomers with water as a reference.

We conducted differential scanning calorimetry (DSC – Discovery DSC, TA instruments) under a nitrogen gas purge to determine glass transition temperatures (T_g) of the latex films. The samples were first equilibrated at −20 °C and followed by a heat/cool/heat cycle with a heating/cooling rate of 10 °C/min between −20 °C and 150 °C. The isothermal steps were applied for 2 min at the top and the bottom temperatures. The midpoint T_g was measured from the second heating curve of each sample. We performed three measurements per sample and reported average values with the standard deviations.

The viscosity of the latexes was measured at room temperature with a Physica MCR 501 (Anton Paar) rheometer. The CP40 cone at a 100 s^{-1} shear rate was used in the measurement.

The latex films were tested with a high-throughput mechanical characterization (HTMECH) instrument [23] to determine the ultimate tensile strength (UTS) and strain at break. The films were deformed biaxially with a 1.25 mm diameter hemispherical indenter normal to the film plane at a speed of 10 mm/s until a rupture occurred. We performed five measurements per sample and presented average values with the standard deviations.

Dynamic mechanical analysis (DMA – Mettler Toledo DMA/SDTA861) was performed to determine the storage and loss moduli of the latex films. Latex samples were cut into rectangular samples about 20 mm long and 3 mm wide. The testing length was 9 mm, and the samples were tested in tension at room temperature within the linear response region of strain. The moduli of the samples were analyzed using a frequency sweep method from 0.1 to 100 Hz.

3. Results and discussion

3.1. Characterization of CNCs

The surface functionalization of mCNC and gmCNC was confirmed by ATR-FTIR spectroscopy (Fig. 2a), water contact angle measurements (Fig. 2b), elemental analysis, and TGA (Fig. 3). In Fig. 2a, FTIR spectra of the CNC samples displayed absorbances at the bands characteristic of cellulose [24]. The wide peak at 3000-3700 cm^{-1} corresponded to stretching vibration bands of the hydroxyl bonds of the hydroxyl groups. The peak at 2900 cm^{-1} was associated with the stretching vibration of C–H bond, whereas the peaks at 1110 cm^{-1}, 1060 cm^{-1}, and 1035 cm^{-1} showed the absorbances due to the vibrations of the C–O bond of carbons 2, 3, and 6. The spectra of mCNC and gmCNC overall kept the identity of the CNC spectra but showed new peaks and changes in the intensities of some absorbances. In the spectrum of mCNC, new peaks at around 1700 cm^{-1} and 1630 cm^{-1} corresponded to C═O and C═C groups, implying the attachment of IEM molecules to the surface of CNCs. Also, mCNC displayed a lower hydroxyl absorbance compared to umCNC. The changes in the spectrum of gmCNC compared to the spectrum of mCNC verified the grafting of BA and MMA monomers. We noted higher absorbances for C═O group at 1700 cm^{-1} and C–O group at 1140 cm^{-1} due to ester groups in the acrylic polymer grafts. Also, the absorbance at 2900 cm^{-1} for alkane C–H stretching was higher in the spectra of gmCNC because of C–H bonds in the attached polymer chains. Furthermore, we did not observe the peak at 1630 cm^{-1} due to C═C.

The water contact angles measured on the CNC films were used to assess the changes in the hydrophilicity of CNCs after the surface

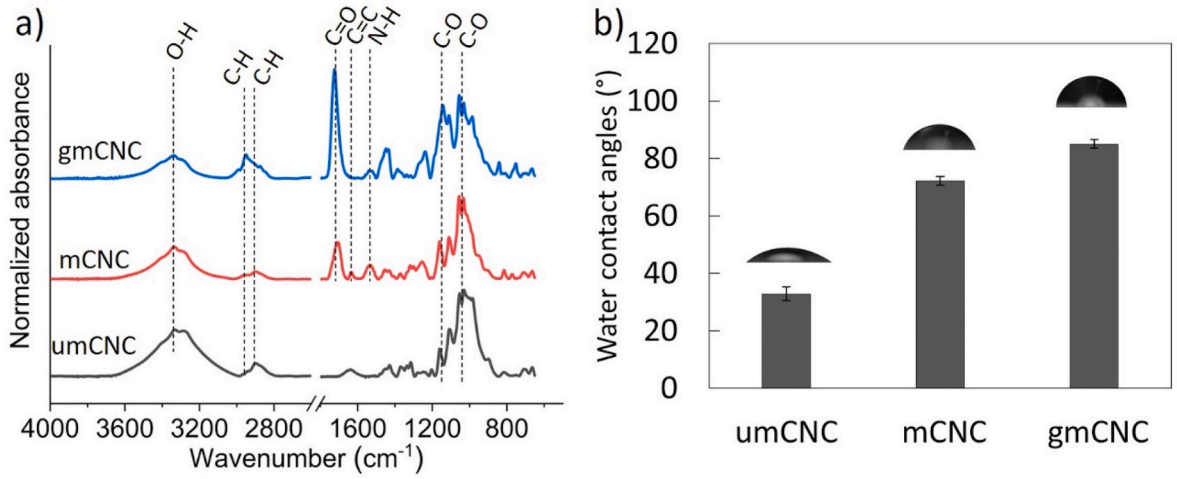

Fig. 2. a) FTIR spectra and b) water contact angle measurements of umCNC, mCNC, and gmCNC.

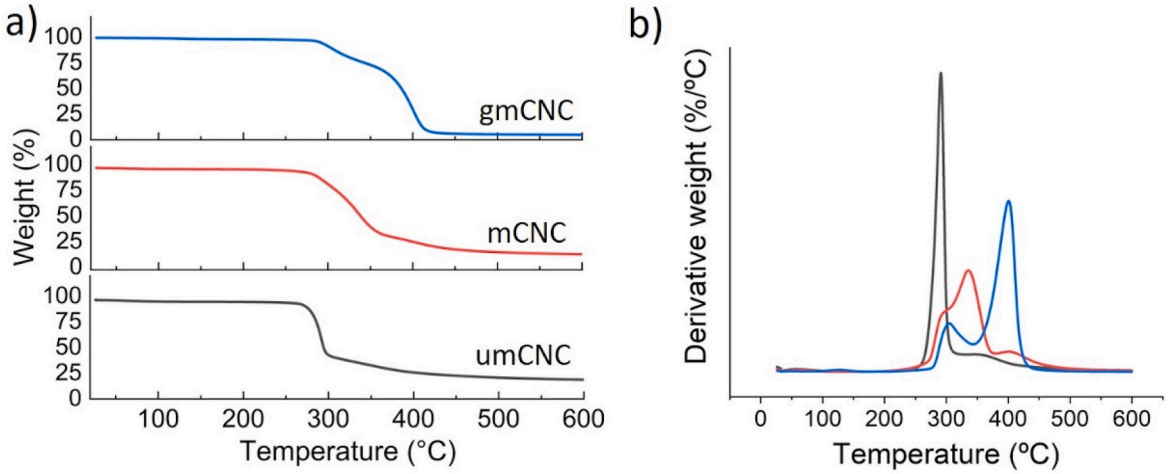

Fig. 3. a) Weight loss curves and b) derivative weight loss curves of umCNC, mCNC and gmCNC.

modifications. Fig. 2b shows the water contact angles on umCNC, mCNC, and gmCNC films. mCNC has reduced hydrophilicity with a contact angle of 72 ± 1° compared to umCNC with a contact angle of 33 ± 2°. This change was expected since the portion of the surface hydroxyls on umCNC reacted with IEM and formed urethane linkages. The water contact angle of gmCNC was measured as 85 ± 2°, higher than the contact angle of mCNC. The further reduction in hydrophilicity of the gmCNC indicated the presence of grafted hydrophobic polymer on the surface of mCNCs.

In Fig. 3, weight loss curves and derivative weight loss curves of CNCs also suggested the success of both surface functionalization on mCNC and gmCNC. The umCNC lost weight in two major steps. The outer layer of umCNCs with sulfate groups began to degrade around 270 °C, and this event was followed by the slower degradation of the crystal interior. The mCNC began to lose weight at around 295 °C, later than the degradation onset of umCNCs. The onset of degradation for mCNCs increased due to covalently attached IEM molecules on the surface of CNCs, which was consistent with previous isocyanate modification reports [25,26]. The mCNC had an additional degradation event in the temperature range of 310–370 °C likely due to the urethane linkages formed between CNC and IEM in the mCNC. The gmCNC degraded in two steps. First, the CNC began to degrade because of low thermal stability of CNCs compared to the grafted acrylic polymer. The subsequent weight loss was attributed to the degradation of the polymer attached to CNC beginning around 330 °C, close to previously reported degradation temperatures of the poly (BA/MMA) copolymer. The weight loss curve of gmCNC was used to estimate the relative wt% of CNC and the attached polymer in the gmCNC. The grafted BA/MMA polymer content was found to be approximately 70 wt%, as shown in Fig. S3.

Elemental analysis of CNC samples resulted in further confirmation of the surface modifications in mCNC and gmCNC. The results of the elemental analysis are given in Table 2. As expected, the umCNC contained no nitrogen (N). In the surface modification of CNC, an IEM molecule forms a urethane linkage containing one N. Therefore, the measured 2.9 wt% N in mCNC and 0.7 wt% N in gmCNC indicate the presence of IEM in the functionalized CNCs. The gmCNC has a lower N

Table 2
Elemental weight percentage composition of umCNC, mCNC and gmCNC.

	Elements wt% ± 0.3 wt%				
	C	H	N	S	O[a]
umCNC	40.6	6.2	0	1.1	52.1
mCNC	45.4	6.1	2.9	0.9	44.7
gmCNC	56.5	7.7	0.7	0.3	34.8

[a] Values calculated content by subtracting the sum of C, H, N, and S from 100%.

composition, a higher C, and a higher H composition compared to mCNC, consistent with the C, H, and O contents added by the grafted polymer chains.

We obtained information about the degree of IEM modification and the grafted polymer by using the results of elemental analysis and the dimensions of the CNCs used in this work. The details of the calculations are given in the calculation section of Supplementary Information. The percent of surface hydroxyls of CNCs reacted with IEM was estimated to be around 65%, corresponding to nearly the limit of maximum surface modification possible [27]. Moreover, the composition of MMA and BA in the grafted polymer was determined as 65 wt% and 35 wt%, respectively. We estimated the number average of molecular weight (M_n) of attached polymer chains as ~1600 g/mol by following the protocol reported by Zhang et al. [28], without chain cleavage. The grafting density was found to be 0.39 chains/nm^2 by using the estimated M_n and the polymer content obtained from TGA.

The morphologies of umCNC, mCNC and gmCNC were characterized by AFM. Fig. 4 shows the representative AFM amplitude images of umCNC, mCNC, and gmCNC. The distributions of the CNC dimensions (length and height) measured from multiple height images are given in Fig. S4. We compared size distributions of umCNC-mCNC and mCNC-gmCNC by using a *t*-test with $\alpha = 0.05$. The length difference between umCNC and mCNC was significant, whereas their heights were found to be similar. On the other hand, the difference in the lengths of mCNC and gmCNC was insignificant; however, the average height of gmCNC statistically increased relative to mCNC due to the polymer chains on the surface of gmCNCs.

The dispersion of CNCs in the monomer phase of the miniemulsion is crucial to maintaining the CNCs inside the monomer droplets during the polymerization. We first investigated the stability of CNCs in the mixture of BA and MMA. Then, we performed partition tests to assess the preference of CNCs for aqueous or monomer phases in a miniemulsion. BA/MMA monomer mixtures containing 1 wt% CNCs were prepared, and water was added to CNC/monomer dispersions. The monomer-to-water ratio was 1:4 as in our miniemulsion procedure, and as a control, we prepared a monomer mixture with no CNCs added. The top picture in Fig. 5 shows the vials containing monomer mixtures. While the monomer mixture with no CNC added was a clear liquid, the mCNC and gmCNC in the monomer mixture resulted in cloudy dispersions. However, the umCNC was not compatible enough with the monomer mixture to form a dispersion and quickly settled to the bottom of the vial. The dispersion stability of mCNC and gmCNC was compared by watching the vials over time to see if any sedimentation occurred. The mCNC began to settle to the bottom of the vial after 5 h, and the aggregates of mCNC sedimented after 24 h (Fig. 6). We did not observe any sedimentation in the gmCNC/monomer dispersion after 24 h. The bottom picture in Fig. 5 shows the vials containing monomer-water phases. The picture was taken 15 min after mixing, allowing CNCs to partition to their preferred phase. The neat monomer mixture phase was on top of the water phase in the first vial. Whereas umCNCs preferred to migrate into the water phase in the second vial, both mCNC and gmCNC partitioned to the monomer phase. The clarity of water phases suggests that the majority of mCNC and gmCNC remained in the monomer mixture.

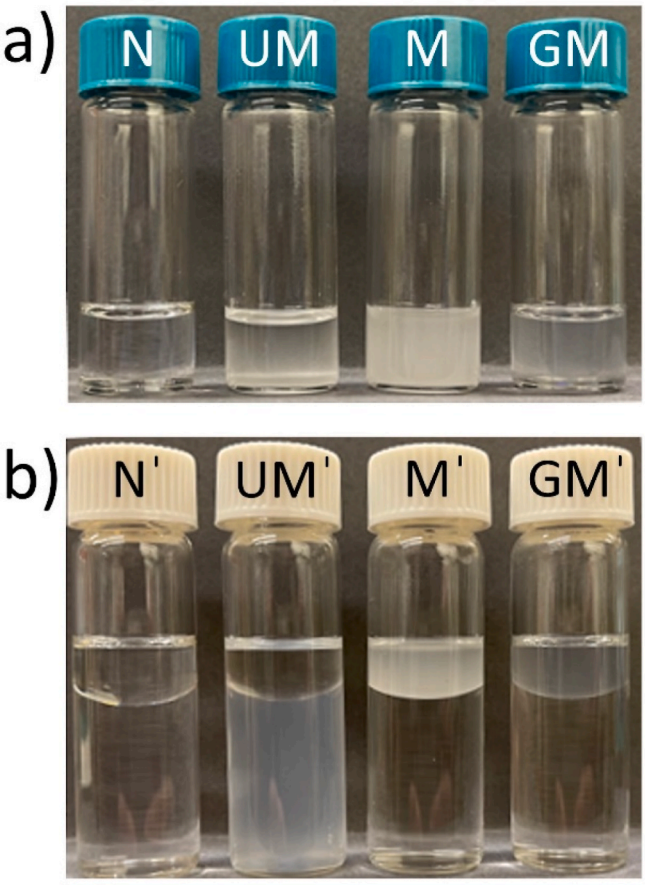

Fig. 5. Photographic images of a) 50 wt% BA – 50 wt% MMA monomer mixture with no CNCs (N),1 wt% umCNCs (UM), 1 wt% mCNCs (M), 1 wt% gmCNCs (GM) and b) corresponding water (bottom) - monomer (top) phases in the vials labelled with a prime symbol.

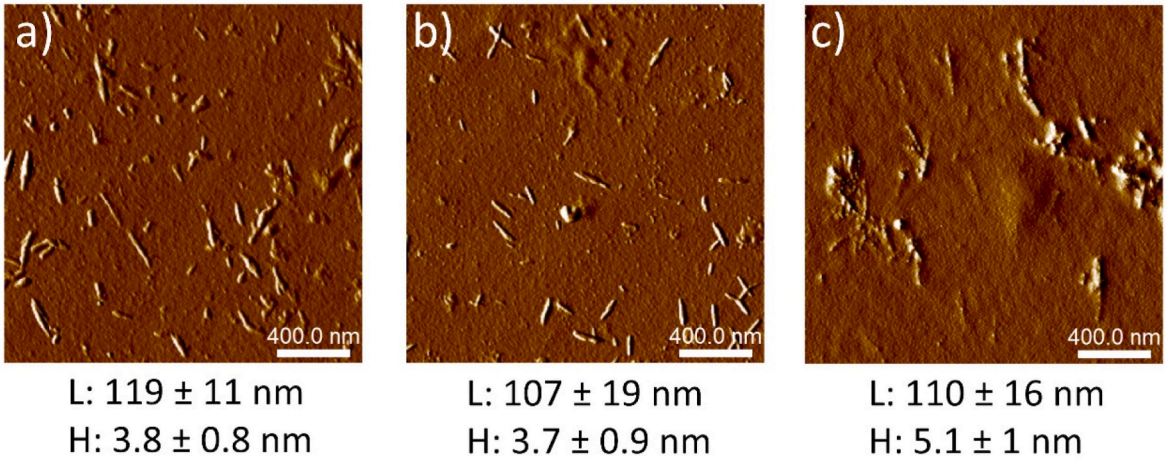

Fig. 4. AFM amplitude images of a) umCNC, b) mCNC, and c) gmCNC.

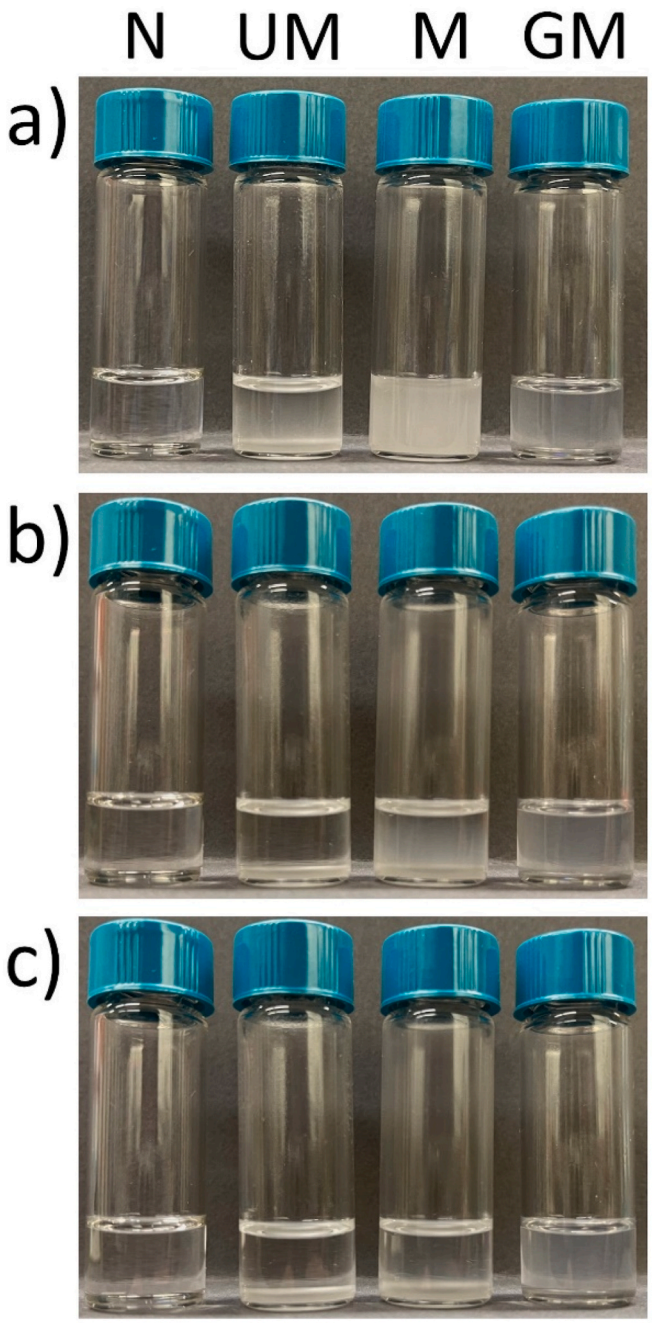

Fig. 6. Photographic images of 50 wt% BA – 50 wt% MMA monomer mixture with no CNCs (N), 1 wt% umCNCs (UM), 1 wt% mCNCs (M), 1 wt% gmCNCs (GM). The pictures were taken after resting a) 5 min, b) 5 h, and c) 24 h.

3.2. Miniemulsion polymerization

3.2.1. Controlling the particle size of the latex

Miniemulsions with the neat BA/MMA monomer mixture were prepared by using different amounts of surfactants to control the particle diameter of the latex. Table 3 summarizes the characteristics of the produced latexes, including particle size, surface tension, coagulum percent, monomer conversion, and pH. We maintained the pH of the latexes in the range of 8–9 by using sodium bicarbonate in conjunction with the KPS initiator. The average particle size of the latexes ranged from 106 to 290 nm. Overall, a lower amount of surfactant led to a larger particle size and a higher surface tension.

An equilibrium exists among the surfactant molecules at the water/air interface, in micelles, in the bulk aqueous phase, and adsorbed at droplet/water interfaces. A higher surface tension measured at the water/air interface of the latex indicates a lower concentration of surfactant present in the aqueous phase. Surface tension measurements ranged from 55 to 62 mN/m, higher than the surface tension measured at CMC of SDBS (35 mN/m in Fig. S5). This result indicates that no micelles were present in any of the latexes, and the surface coverages of the particles were incomplete. The surface tension increased with decreasing surfactant concentration, as expected. The surface coverage decreased with decreasing surfactant content and increasing particle size; with less surface coverage, more particles are prone to coagulation [29]. Also, large particles tend to coagulate due to Stokes law settling, consistent with the observed increasing amount of coagulum with decreasing surfactant concentration. Based on the monomer conversion calculations, a slower polymerization occurred when a lower surfactant concentration was used. This was expected because less surfactant results in a smaller number of monomer droplets that are larger in size and consequently a lower particle number causing a slower polymerization [30].

Table 3
Effects of the variation in the surfactant concentration on the characteristics of the latexes.

Surfactant concentration (mM)	Average particle size (nm)	Surface tension (mN/m)	Coagulum (%)	Monomer conversion (%)	pH
0.81	290 ± 4	62.6 ± 0.08	4.40	79.0	8.42
1.61	205 ± 3	61.6 ± 0.06	2.44	85.4	8.37
3.23	144 ± 4	59.8 ± 0.08	1.96	89.7	8.44
4.85	121 ± 2	58.6 ± 0.04	1.45	91.3	8.46
7.28	106 ± 3	55.4 ± 0.04	1.15	92.4	8.76

3.2.2. Incorporating CNCs into the latex

We selected two different surfactant concentrations (0.81 mM and 2.42 mM) to be used in the latex formulations including CNCs, in order to obtain particle sizes larger than the length of the CNCs. The latexes were denoted as L-X-Y-Z where X represents the concentration of the surfactant (mM) and Y stands for the type of CNCs used in the preparation of latexes while Z is for the CNC loading. Fig. 7 shows the measurements of average particle size and zeta potential of all latexes. The hydrodynamic diameters measured in all latexes (Fig. 7a) were in the range of 186–430 nm, with polydispersity indexes less than 0.1. As expected, the latexes with a lower surfactant concentration had larger particle sizes compared to the average sizes obtained in the case of high surfactant concentration. For both surfactant concentrations, the size of L-umCNC and L-mCNC increased with increasing CNC loading; however, the size of L-0.81-gmCNC decreased and the size of L-2.42-gmCNC remained unchanged with increasing CNC loading. Elmabrouk et al. [33] previously observed an increase in the particle size of poly(styrene-*co*-hexylacrylate) latex particles when umCNCs were loaded to the aqueous phase via miniemulsion polymerization. The result was attributed to particle agglomeration driven by umCNCs during the polymerization.

Fig. 7b displays the zeta potential measurements. The zeta potentials of all latexes were negative due to the anionic surfactants at the surface of latex particles. Also, all measured zeta potentials were more negative than −40 mV, indicating good colloidal stability. In general, the zeta potential of L-Neat and L-gmCNC had an insignificant difference (by *t*-test with $\alpha = 0.05$), whereas the zeta potential of L-mCNC and L-umCNC were less negative compared to L-Neat and L-gmCNC.

Table 4 provides the properties of the synthesized latexes such as surface tension, coagulum percent, monomer conversion, pH, and

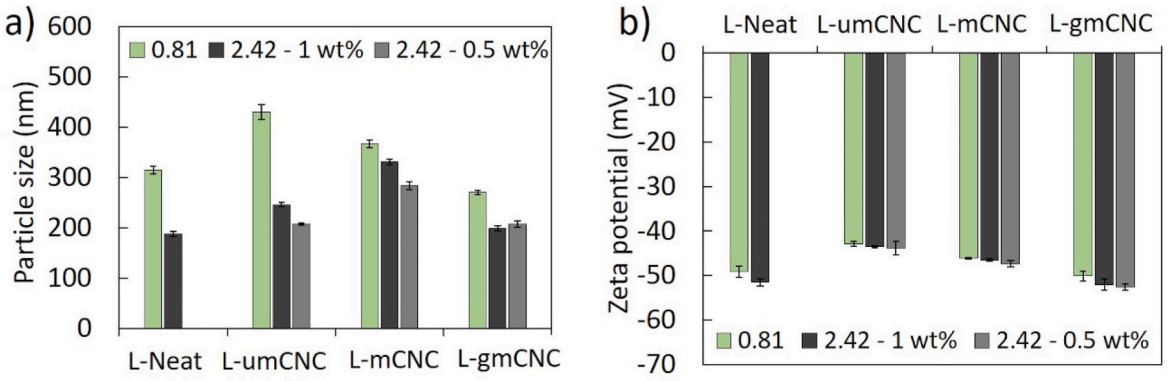

Fig. 7. a) Average particle size and b) zeta potential of acrylic latexes.

Table 4
Summary of latex properties and T_g of the resulting latex films.

Latex samples	Surface tension (mN/m)	Coagulum (%)	Monomer conversion (%)	pH	Viscosity (cp)	T_g (°C)
L-0.81-Neat	55.9	2.92	88.5	7.86	1.74	22 ± 0.4
L-0.81-umCNC-1 wt%	54.6 ± 0.7	2.41	86.7	7.46	7.87	21 ± 2
L-0.81-mCNC-1 wt%	47.9 ± 0.6	3.04	83.2	7.73	1.60	18 ± 0.3
L-0.81-gmCNC-1 wt%	54.6 ± 0.4	3.18	83.5	7.60	1.63	20 ± 0.7
L-2.42-Neat	54.7 ± 0.4	2.19	90.3	7.54	1.76	22 ± 0.3
L-2.42-umCNC-1 wt%	53.1 ± 0.8	2.08	88.1	7.71	7.01	21 ± 1
L-2.42-umCNC-0.5 wt%	53.7 ± 0.2	3.05	87.9	7.88	3.17	22 ± 0.4
L-2.42-mCNC-1 wt%	45.4 ± 0.4	2.70	84.7	7.73	1.65	19 ± 1
L-2.42-mCNC-0.5 wt%	45.3 ± 0.2	2.17	85.3	7.77	1.65	21 ± 1
L-2.42-gmCNC-1 wt%	53.2 ± 0.4	3.17	85.3	7.81	1.72	20 ± 1
L-2.42-gmCNC-0.5 wt%	52.9 ± 0.5	3.30	86.9	7.79	1.60	20 ± 1

viscosity and also lists the T_g of the resulting latex films. The pH of all latexes was maintained within the same range (pH = 7–8). The surface tensions of latexes containing less surfactant were slightly higher than the latexes with higher surfactant concentration. The latexes prepared with mCNCs (L-0.81-mCNC-1 wt%, L-2.42-mCNC-1 wt%, and L-2.42-mCNC-0.5 wt%) had a lower surface tension (45–48 mN/m) relative to the surface tension of the rest of the samples, ranging from 53 to 55 mN/m. The mechanism causing the decrease in the surface tension is not well-understood. We expect that mCNCs concentrated at the monomer/water interface during polymerization, based on the observation from the partition tests over time. The mCNCs were not as compatible with the water phase compared to umCNCs or with the monomer phase compared to gmCNCs. This insufficient compatibility with both phases may cause migration of mCNCs to monomer droplet-water interfaces, which could displace surfactant from droplets. This is consistent with the reduction in latex surface tension in the mCNC samples, compared to umCNC and gmCNC in Table 1. Reduced surface tension implies a greater concentration of surfactant at the water-air interface, requiring its migration from the droplet-water interface. With reduced surfactant coverage, some monomer droplets could coagulate during the polymerization. The latexes with higher surfactant concentration (2.42 mM) resulted in slightly higher monomer conversions compared to the latexes with a lower surfactant concentration (0.81 mM). This result was anticipated due to the smaller particle sizes expected in the latexes prepared with a higher surfactant concentration. However, the monomer conversions were slightly lower when we include CNCs in the latex synthesis compared to the conversions obtained in the neat latexes.

We obtained latex coagulum levels ranging from 2.1 to 3.3% of total solid content with no notable differences between samples. The latex films and the coagula were characterized by ATR-FTIR and the spectra of the samples were given in Fig. S6. While the spectra of all latex films show the same fingerprint, the coagula obtained from the latexes with mCNCs were different. The coagula of L-0.81-mCNC-1 wt%, L-2.42-mCNC-1 wt%, and L-2.42-mCNC-0.5 wt% exhibited some of the characteristic peaks of CNC; for example, hydroxyl stretching at 3000-3700 cm^{-1}. Also, we observed the peaks at 1060 cm^{-1} and 1035 cm^{-1} corresponding to the C–O bond of carbons 3 and 6 of a CNC. These peaks suggested the tendency of mCNCs to concentrate in the coagulum during the polymerization. The presence of mCNCs in the coagula was further verified by elemental analysis.

In Table S1, the results of the elemental analysis were provided for carbon (C), hydrogen (H) and nitrogen (N) in all latex films and coagula. Samples were dominantly comprised of C, H, and O because of the elemental composition of the latexes (copolymer of MMA-$C_5H_8O_2$ and BA-$C_7H_{12}O_2$). The mCNC and gmCNC contained N because of the NCO moiety of IEM attached to CNCs. However, no N content was detected in any latex film. We did not expect N in L-Neat and L-umCNC samples and the N would be only 0.03 wt% and 0.006 wt% for 1 wt% mCNC and 1 wt % gmCNC loaded latexes, respectively, by assuming a homogeneous distribution of CNCs within the latex system. These expected N contents in L-mCNC and L-gmCNC samples are significantly lower than the detection uncertainty (±0.3 wt%) of the method used in the elemental analysis. On the other hand, the coagulum of L-0.81-mCNC-1 wt%, L-2.42-mCNC-1 wt%, and L-2.42-mCNC-0.5 wt% contained 0.95 wt%, 0.75 wt% and 0.5 wt% N, respectively. Consistent with the mCNC loadings, N wt% detected in the coagulum of L-2.42-mCNC-0.5 wt% was lower than the N in the coagulum of L-2.42-mCNC-1 wt%. When we assumed the coagulation of all mCNCs, the N content in the coagulum would be approximately 1 wt% N for 1 wt% mCNC-added latexes. These numbers indicated that nearly all mCNCs coagulated at the end of the polymerization, and the latex had almost no mCNC. For 1 wt% gmCNC-added latex coagulum, the N content in the coagulum was calculated as 0.21 wt% by assuming the coagulation of all loaded gmCNCs. Therefore, N content in the coagula of L-0.81-gmCNC-1 wt%, L-2.42-gmCNC-1 wt %, and L-2.42-gmCNC-0.5 wt% may not be detectable due to the sensitivity of the elemental analysis technique.

Table 4 also shows the viscosity measurement of the latexes. The viscosities of latexes prepared with umCNC (L-0.81-umCNC-1 wt%, L-

2.42-umCNC-1 wt%, and L-2.42-umCNC-0.5 wt%) were substantially higher when compared to the rest of the samples having similar viscosities. This result can be associated with the shear thinning nature of CNCs, and the presence of a higher concentration of dispersed entities (particles and CNCs), suggesting the existence of umCNCs in the aqueous phase.

Overall, both the results of FTIR and elemental analysis showed the presence of mCNCs in the coagulum of the latexes prepared with mCNC. However, we could neither confirm nor contest the presence of gmCNCs in the coagula of the latexes synthesized with gmCNC because of the sensitivity of the techniques used. The gmCNCs clearly have better compatibility with the monomers compared to mCNCs and umCNCs, as shown in Figs. 5 and 6. The surface tension and viscosity measurements support the encapsulation of gmCNCs inside the monomer droplets, whereas umCNCs prefer the water phase. The insufficient compatibility of mCNCs with either the water phase or monomer phase likely leads to their coagulation, preventing the use of mCNCs as a comonomer.

T_g of latex films is an important property to understand the difference in the polymer segmental mobilities and copolymer-filler interactions. We measured T_g of the latex films in the range of 18–22 °C. This range of T_g values can result from the small changes in the coagulum percentages and monomer conversions. Polymer composition is impacted by monomer conversion because of the difference in reactivities of the two monomers used. Although BA is more reactive in homopolymerization than MMA, the reactivity ratios ($r_{BA} = 2.55$ and $r_{MMA} = 0.36$) indicate that the MMA will be consumed at a much higher rate than the BA in copolymerization [31] and a variation in the polymer composition (composition drift) is expected due to the batch process used. Therefore, it is difficult to draw a clear conclusion about the effect of the CNC type and loading on polymer mobility. However, we observed slightly lower T_g in the latex films prepared with mCNC (found to be statistically different from other latex films by t-test with $\alpha = 0.05$). The mCNCs can play a role in the composition drift because the vinyl groups on the surface of mCNCs are available for polymerization with a portion of monomers. IEMs on the surface of mCNC tend to react more favorably with MMA than BA ($r_{IEM} = 1.19$ and $r_{MMA} = 0.84$; $r_{IEM} = 2.50$ and $r_{MMA} = 0.40$) [32]. Therefore, the unreacted BA composition remaining for latex synthesis increases while the mCNCs coagulated, lowering the T_g of the resulting latex film.

The latex particles were imaged by AFM to analyze the particle morphologies in the latexes and to identify the location of the CNCs. AFM amplitude images of the latex particles are given in Fig. 8. In some images, latex particles are partially coalesced due to the fact that the T_g of the polymers is close to the ambient temperature. As expected, we observed only spherical polymer particles in the neat latex samples (Fig. 8a and e). Regardless of the surfactant concentration used, latexes prepared with umCNC contained rod-like CNCs outside the latex particles (Fig. 8b and f) even though umCNCs were initially incorporated into the monomer phase. We did not observe any rod-like particles in L-0.81-mCNC-1 wt% and L-2.42-mCNC-1 wt% (Fig. 8c and g), supporting our conclusion from the previous characterization about the presence of mCNCs in the coagula as opposed to the latex. Fig. 8d and h show the particle morphologies of latexes prepared with gmCNC (L-0.81-gmCNC-1 wt% and L-2.42-gmCNC-1 wt%). The gmCNCs were not observed outside of the latex particles, unlike umCNCs. We recognized faint rod-like features on/in the particles of L-0.81-gmCNC-1 wt% and L-2.42-gmCNC-1 wt%, suggesting the presence of gmCNCs partially on the outside or buried inside the acrylic particles. To better demonstrate the particle morphology observed in gmCNC-added latex samples, Fig. 9 displays AFM height, amplitude, and phase images of the region marked with a white square in Fig. 8h. In the phase image, Fig. 9c, rod-like features have a light color similar to the hard substrate, compared to the darker color of the polymer particles. This observation supports the interpretation that hard gmCNCs are located on the surface of latex particles.

Mechanical testing of the final latex films was performed by a biaxial film tensile test (HTMECH) and DMA. We obtained tensile strength and strain at break from HTMECH, and the results are shown in Fig. 10. The tensile strength and strain at break values of all latex films were not statistically different from each other (by t-test with $\alpha = 0.05$). The tensile strength of the latex films was around 6–7 MPa, while the strain at break was about 250%.

Frequency scan tests were performed with DMA at room temperature to understand the impact of CNC type or concentration on the moduli of the latex films. The storage modulus measurements are given in Fig. 11. The loss modulus and tan δ values are provided in Table S2. The storage moduli of L-2.42-umCNC-0.5 wt% and L-2.42-umCNC-1 wt% were slightly higher than the moduli of L-2.42-Neat, though at some higher

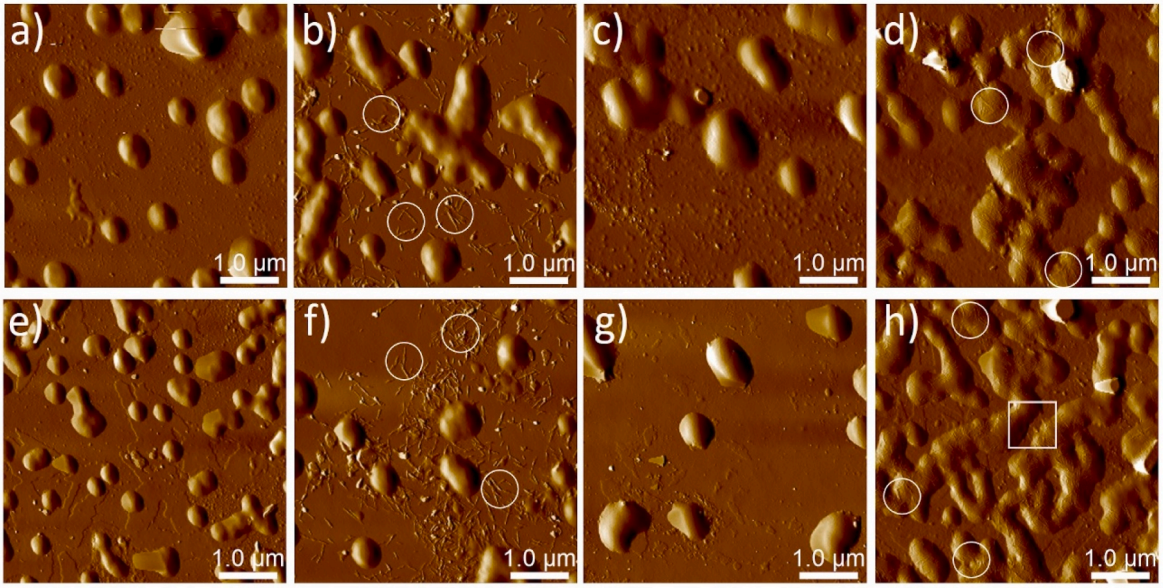

Fig. 8. AFM amplitude images of particle morphology in the latexes: a) L-0.81-Neat, b) L-0.81-umCNC-1 wt%, c) L-0.81-mCNC-1 wt%, d) L-0.81-gmCNC-1 wt%, e) L-2.42-Neat, f) L-2.42-umCNC-1 wt%, g) L-2.42-mCNC-1 wt%, and h) L-2.42-gmCNC-1 wt%. Circles show CNCs outside and inside the latex particles. The square region is shown in Fig. 9.

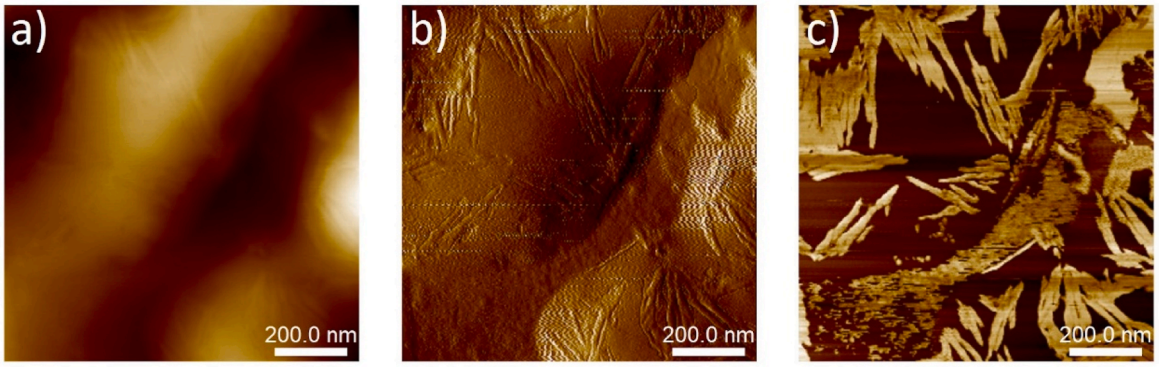

Fig. 9. AFM images (a: height, b: amplitude, and c: phase) of L-2.42-gmCNC-1 wt% with 1 μm scan size showing the region marked with a white square in Fig. 8h.

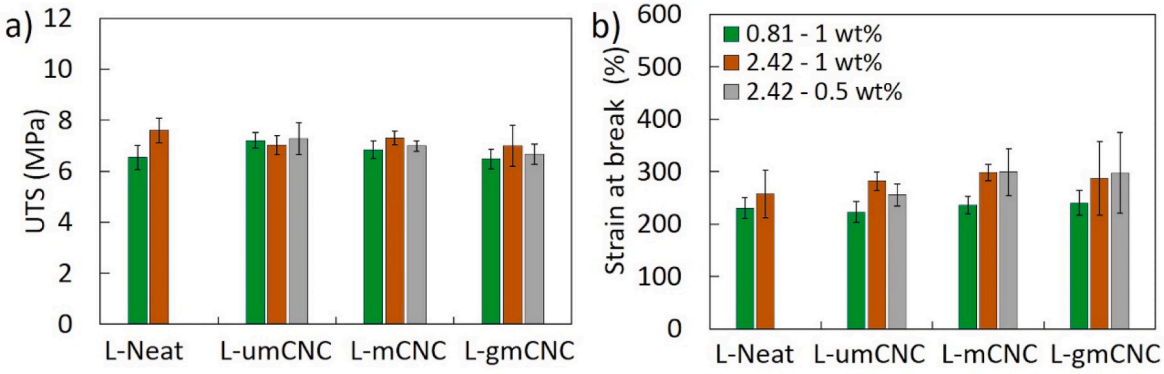

Fig. 10. a) UTS and b) strain at break of the latex films.

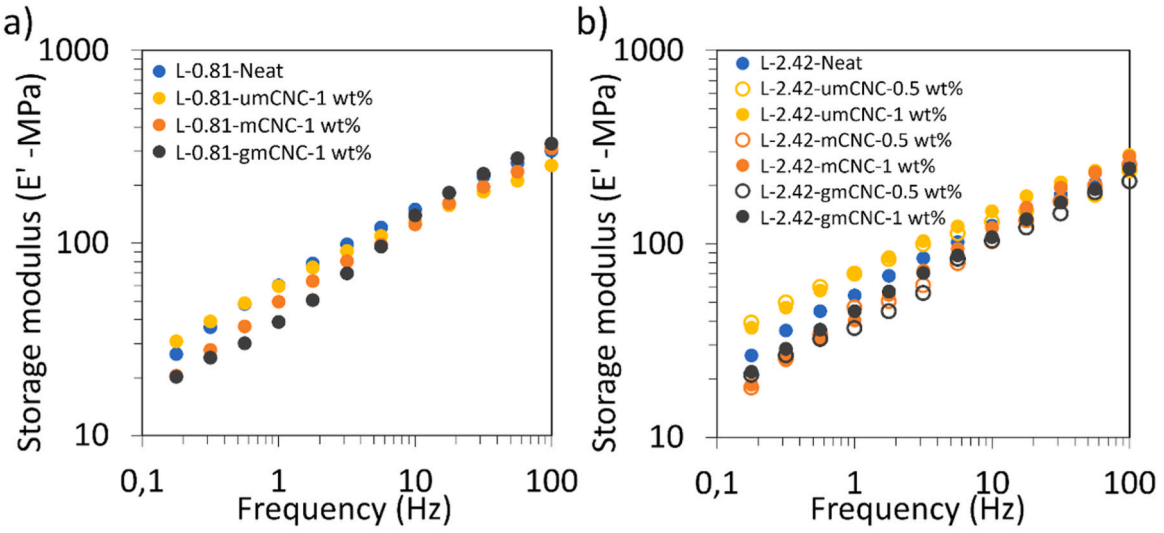

Fig. 11. Storage modulus (MPa) of a) L-0.81 and b) L-2.42 samples with different CNC types and loadings as a function of frequency (in the linear regime at 25 °C).

frequencies this trend was reversed for the 0.5 loading. Conversely, the moduli of L-2.42-mCNC and L-2.42-gmCNC samples (both 0.5 wt% and 1 wt%) were slightly lower than the moduli of L-2.42-Neat at most frequencies. For example, at 1 Hz, the modulus of L-2.42-Neat was 54 MPa, while the moduli of L-2.42-umCNC-1 wt%, L-2.42-mCNC-1 wt%, and L-2.42-gmCNC-1 wt% were 69 MPa, 40 MPa, and 44 MPa, respectively. These slight changes in the modulus values may not necessarily be a function of CNC type only, because minor differences in the T_g of the related latex films (Table 4) could affect the storage moduli. Also, CNC concentration did not remain at 1 wt% loading in all latex films. For example, mCNC coagulated during polymerization and could not be incorporated into the latex films. In addition, the encapsulation efficiency of gmCNCs is unknown, although they appear to be present in the particles in Figs. 8 and 9. Because of these factors affecting the moduli and the proximity of the measured values, it is difficult to draw conclusions about the differences between samples.

In general, the mechanical properties in the CNC loaded latex films were not markedly different from those of the neat latex films. This

outcome was expected for the latexes prepared with mCNCs because mCNCs were mostly detected in the coagula and not in the films formed from products latex particles. The outcome was also expected for the latex films prepared with umCNC due to the tendency of CNCs in the aqueous phase to aggregate during film formation, thus reducing their effectiveness [16]. No significant mechanical reinforcement was observed for umCNC/waterborne acrylic composites at a loading of 1 wt % CNC. However, we expected some difference in the mechanical properties of gmCNC-added samples because the encapsulation of the filler is anticipated to result in a homogenous distribution of the filler in the polymer matrix [34,35] (see Fig. 1). There are several possible explanations for the inability to enhance the mechanical properties with gmCNCs. The 1 wt% loading of gmCNCs may not sufficient to enhance the mechanical performance of the resulting films. If the neat film were softer, a 1 wt% loading might make a difference in the mechanical properties, due to the larger modulus contrast between the components. For example, Yu et al. [19] measured the shear moduli (G′ and G") of CNC loaded (1 wt%) acrylic PSAs (either outside or inside the polymer particles) as a function of frequency by using a rheometer. The reinforcing effect of CNCs was observed where the G′ values of all PSAs were lower than 0.3 MPa. The gmCNCs in this study contain only 30 wt% CNC, with the balance being the grafted copolymer, so the 1 wt% loading represents 0.3 wt% CNC at most. A higher CNC content may have a larger effect on mechanical performance; however, we observed significant coagulation (coagulum >10 wt%) when 3 wt% gmCNC was incorporated into the monomer phase of miniemulsion. This result may be associated with the increased viscosity of the monomer phase with increasing CNC content. Increasing viscosity of the monomer phase limits the ability to form small droplets under fixed shear, preventing generation of a miniemulsion [35].

4. Conclusions

This study emphasizes how the compatibility of CNCs with the monomer phase is essential for a successful encapsulation in miniemulsion polymerizations of acrylic comonomers. This paper explored the use of acryloyl- and butylacrylate/methylmethacrylate-copolymer-grafted CNCs in miniemultion polymerizations of butyl- and methylmethacrylate comonomers, carried out with industrially relevant features, including use of a nonpolar costabilizer and water soluble initiator. We demonstrate that the grafted polymer-modified CNCs can be physically incorporated into the copolymer latex particles. In contrast, we found that umCNCs migrated from monomer droplets into the aqueous phase. We investigated whether or not the presence of a reactive (-C═C- containing) acryloyl moiety enables the modified CNC to serve as a comonomer, that reacts into the acrylic chains chemically. The mCNCs were found in the latex coagulum, suggesting that they did not possess long-term stability in either the aqueous or monomer phase. The gmCNCs were more compatible with acrylic monomers relative to mCNCs. However, no major changes were observed in the mechanical performance of the latexes prepared with different types of CNCs relative to neat latex, which is likely due to the relatively low loadings achieved. This work encourages the study of the optimization of polymer grafting and CNC/monomer compatibility to better understand their incorporation via miniemulsion polymerization. Overall, we believe that the knowledge provided here provide some design guidelines for the incorporation of organic nanoparticles similar to CNCs into the latex particles.

CRediT authorship contribution statement

Ezgi M. Dogan-Guner: Conceptualization, Methodology, Validation, Formal analysis, Investigation, Visualization, Writing – original draft, Writing – review & editing. **F. Joseph Schork:** Conceptualization, Supervision, Writing – review & editing. **Stan Brownell:** Conceptualization, Resources, Writing – review & editing. **Gregory T. Schueneman:** Conceptualization, Resources, Writing – review & editing. **Meisha L. Shofner:** Conceptualization, Supervision, Writing – review & editing. **J. Carson Meredith:** Conceptualization, Supervision, Writing – review & editing.

Declaration of competing interest

The authors declare that they have no known competing financial interests or personal relationships that could have appeared to influence the work reported in this paper.

Acknowledgments

This research was financially supported by the P^{3}Nano program in the US Endowment for Forestry and Communities. The authors of this paper would like to thank the USDA Forest Service Forest Products Laboratory (FPL) for their collaboration. This work was performed in part at the Georgia Tech Institute for Electronics and Nanotechnology, a member of the National Nanotechnology Coordinated Infrastructure, which is supported by the National Science Foundation (Grant ECCS-2025462).

Appendix A. Supplementary data

Supplementary data to this article can be found online at https://doi.org/10.1016/j.polymer.2021.124488.

References

[1] A.J. DeFusco, K.C. Sehgal, D.R. Bassett, Overview of uses of polymer latexes, in: J. M. Asua (Ed.), Polymeric Dispersions: Principles and Applications, Springer Netherlands, Dordrecht, 1997, pp. 379–396, https://doi.org/10.1007/978-94-011-5512-0_25.
[2] B. Richey, M. Burch, Applications for decorative and protective coatings, in: D. Urban, K. Takamura (Eds.), Polymer Dispersions and Their Industrial Applications, Wiley-VCH Verlag GmbH & Co. KGaA, Weinheim, 2002, pp. 123–161, https://doi.org/10.1002/3527600582.ch6.
[3] P.A. Lovell, F.J. Schork, Fundamentals of emulsion polymerization, Biomacromolecules 21 (2020) 4396–4441, https://doi.org/10.1021/acs.biomac.0c00769.
[4] M. Antonietti, K. Landfester, Polyreactions in miniemulsions, Prog. Polym. Sci. 27 (2002) 689–757, https://doi.org/10.1016/S0079-6700(01)00051-X.
[5] L.L. Hecht, C. Wagner, K. Landfester, H.P. Schuchmann, Surfactant concentration regime in miniemulsion polymerization for the formation of MMA nanodroplets by high-pressure homogenization, Langmuir 27 (2011) 2279–2285, https://doi.org/10.1021/la104480s.
[6] K. Landfester, N. Bechthold, F. Tiarks, M. Antonietti, Formulation and stability mechanisms of polymerizable miniemulsions, Macromolecules 32 (1999) 5222–5228, https://doi.org/10.1021/ma990299+.
[7] S. Theisinger, K. Schoeller, B. Osborn, M. Sarkar, K. Landfester, Encapsulation of a fragrance via miniemulsion polymerization for temperature-controlled release, Macromol. Chem. Phys. 210 (2009) 411–420, https://doi.org/10.1002/macp.200800499.
[8] H.J. Barraza, F. Pompeo, E.A. O'Rea, D.E. Resasco, SWNT-filled thermoplastic and elastomeric composites prepared by miniemulsion polymerization, Nano Lett. 2 (2002) 797–802, https://doi.org/10.1021/nl0256208.
[9] H. Han, J. Lee, D.W. Park, S.E. Shim, Surface modification of carbon black by oleic acid for miniemulsion polymerization of styrene, Macromol. Res. 18 (2010) 435–441, https://doi.org/10.1007/s13233-010-0505-1.
[10] F. Tiarks, K. Landfester, M. Antonietti, Silica nanoparticles as surfactants and fillers for latexes made by miniemulsion polymerization, Langmuir 17 (2001) 5775–5780, https://doi.org/10.1021/la010445g.
[11] S.-W. Zhang, S.-X. Zhou, Y.-M. Weng, L.-M. Wu, Synthesis of SiO2/polystyrene nanocomposite particles via miniemulsion polymerization, Langmuir 21 (2005) 2124–2128, https://doi.org/10.1021/la047652b.
[12] B. Erdem, E.D. Sudol, V.L. Dimonie, M.S. El-Aasser, Encapsulation of inorganic particles via miniemulsion polymerization. III. Characterization of encapsulation, J. Polym. Sci. Polym. Chem. 38 (2000) 4441–4450, https://doi.org/10.1002/1099-0518(20001215)38:24<4441::AID-POLA130>3.0.CO;2-U.
[13] X. Liu, Y. Guan, Z. Ma, H. Liu, Surface modification and characterization of magnetic polymer nanospheres prepared by miniemulsion polymerization, Langmuir 20 (2004) 10278–10282, https://doi.org/10.1021/la0491908.
[14] D.J. Voorn, W. Ming, A.M. van Herk, Clay platelets encapsulated inside latex particles, Macromolecules 39 (2006) 4654–4656, https://doi.org/10.1021/ma060900l.
[15] C.K. Weiss, K. Landfester, Miniemulsion polymerization as a means to encapsulate organic and inorganic materials, in: A.M. van Herk, K. Landfester (Eds.), Hybrid

Latex Particles: Preparation with (Mini)emulsion Polymerization, Springer Berlin Heidelberg, Berlin, Heidelberg, 2010, pp. 185–236, https://doi.org/10.1007/12_2010_61.
[16] E.M. Dogan-Guner, S. Brownell, G.T. Schueneman, M.L. Shofner, J.C. Meredith, Enabling zero added-coalescent waterborne acrylic coatings with cellulose nanocrystals, Prog. Org. Coat. 150 (2021) 105969, https://doi.org/10.1016/j.porgcoat.2020.105969.
[17] E. Limousin, I. Rafaniello, T. Schäfer, N. Ballard, J.M. Asua, Linking film structure and mechanical properties in nanocomposite films formed from dispersions of cellulose nanocrystals and acrylic latexes, Langmuir 36 (2020) 2052–2062, https://doi.org/10.1021/acs.langmuir.9b03861.
[18] S.A. Kedzior, M. Kiriakou, E. Niinivaara, M.A. Dubé, C. Fraschini, R.M. Berry, E. D. Cranston, Incorporating cellulose nanocrystals into the core of polymer latex particles via polymer grafting, ACS Macro Lett. 7 (2018) 990–996, https://doi.org/10.1021/acsmacrolett.8b00334.
[19] Q. Yu, W. Yang, Q. Wang, W. Dong, M. Du, P. Ma, Functionalization of cellulose nanocrystals with γ-MPS and its effect on the adhesive behavior of acrylic pressure sensitive adhesives, Carbohydr. Polym. 217 (2019) 168–177, https://doi.org/10.1016/j.carbpol.2019.04.049.
[20] E. Lizundia, E. Meaurio, J.L. Vilas, Chapter 3 - grafting of cellulose nanocrystals, in: D. Puglia, E. Fortunati, J.M. Kenny (Eds.), Multifunctional Polymeric Nanocomposites Based on Cellulosic Reinforcements, William Andrew Publishing, 2016, pp. 61–113, https://doi.org/10.1016/B978-0-323-44248-0.00003-1.
[21] T. Leng, Cellulose Nanocrystals: Particle Size Distribution and Dispersion in Polymer Composites, MSc thesis, University of Ottowa, 2016.
[22] A. Brinkmann, M. Chen, M. Couillard, Z.J. Jakubek, T. Leng, L.J. Johnston, Correlating cellulose nanocrystal particle size and surface area, Langmuir 32 (2016) 6105–6114, https://doi.org/10.1021/acs.langmuir.6b01376.
[23] J.-L. Sormana, S. Chattopadhyay, J.C. Meredith, High-throughput mechanical characterization of free-standing polymer films, Rev. Sci. Instrum. 76 (2005), 062214, https://doi.org/10.1063/1.1926967.
[24] E.J. Foster, R.J. Moon, U.P. Agarwal, M.J. Bortner, J. Bras, S. Camarero-Espinosa, K.J. Chan, M.J.D. Clift, E.D. Cranston, S.J. Eichhorn, D.M. Fox, W.Y. Hamad, L. Heux, B. Jean, M. Korey, W. Nieh, K.J. Ong, M.S. Reid, S. Renneckar, R. Roberts, J.A. Shatkin, J. Simonsen, K. Stinson-Bagby, N. Wanasekara, J. Youngblood, Current characterization methods for cellulose nanomaterials, Chem. Soc. Rev. 47 (2018) 2609–2679, https://doi.org/10.1039/C6CS00895J.
[25] N.M. Girouard, S. Xu, G.T. Schueneman, M.L. Shofner, J.C. Meredith, Site-selective modification of cellulose nanocrystals with isophorone diisocyanate and formation of polyurethane-CNC composites, ACS Appl. Mater. Interfaces 8 (2016) 1458–1467, https://doi.org/10.1021/acsami.5b10723.
[26] Z. Qu, G.T. Schueneman, M.L. Shofner, J.C. Meredith, Acrylic functionalization of cellulose nanocrystals with 2-isocyanatoethyl methacrylate and formation of composites with poly(methyl methacrylate), ACS Omega 5 (2020) 31092–31099, https://doi.org/10.1021/acsomega.0c04246.
[27] S. Eyley, W. Thielemans, Surface modification of cellulose nanocrystals, Nanoscale 6 (2014) 7764–7779, https://doi.org/10.1039/C4NR01756K.
[28] Z. Zhang, K.C. Tam, G. Sèbe, X. Wang, Convenient characterization of polymers grafted on cellulose nanocrystals via SI-ATRP without chain cleavage, Carbohydr. Polym. 199 (2018) 603–609, https://doi.org/10.1016/j.carbpol.2018.07.060.
[29] V. Dimonie, D. Sudol, M. El-Aasser, Role of surfactants in emulsion polymerization polymers by design, Rev. Chim. 59 (2008) 1218–1221, https://doi.org/10.37358/RC.08.11.2005.
[30] K. Fontenot, F.J. Schork, Batch polymerization of methyl methacrylate in mini/macroemulsions, J. Appl. Polym. Sci. 49 (1993) 633–655, https://doi.org/10.1002/app.1993.070490410.
[31] M.A. Bradley, S.W. Prescott, H.A.S. Schoonbrood, K. Landfester, F. Grieser, Miniemulsion copolymerization of methyl methacrylate and butyl acrylate by ultrasonic initiation, Macromolecules 38 (2005) 6346–6351, https://doi.org/10.1021/ma0473622.
[32] C.C. Chappelow, T.J. Byerley, C.S. Pinzino, F. Millich, J.D. Eick, Design and development of isocyanatoacrylates as dental adhesives, J. Dent. Res. 75 (1996) 761–767, https://doi.org/10.1177/00220345960750020501.
[33] A.B. Elmabrouk, T. Wim, A. Dufresne, S. Boufi, Preparation of poly(styrene-co-hexylacrylate)/cellulose whiskers nanocomposites via miniemulsion polymerization, J. Appl. Polym. Sci. 114 (2009) 2946–2955, https://doi.org/10.1002/app.30886.
[34] A.M. van Herk, Encapsulation with conventional emulsion polymerization, in: S. Kobayashi, K. Müllen (Eds.), Encyclopedia of Polymeric Nanomaterials, Springer Berlin Heidelberg, Berlin, Heidelberg, 2021, pp. 1–6, https://doi.org/10.1007/978-3-642-36199-9_260-1.
[35] M. Paulis, J.R. Leiza, Encapsulation with miniemulsion polymerization, in: S. Kobayashi, K. Müllen (Eds.), Encyclopedia of Polymeric Nanomaterials, Springer, Verlag Berlin Heidelberg, 2014, https://doi.org/10.1007/978-3-642-36199-9_261-1.